Journal of Applied Polymer Science

Synthesis and Properties of Magnetic Sensitive Shape Memory Fe_3O_4/Poly(ε-caprolactone)-Polyurethane Nanocomposites

Yan Cai,[1] Ji-Sen Jiang,[1] Bing Zheng,[1] Mei-Ran Xie[2]

[1]Department of Physics, Center of Functional Nanomateriels and Devices, East China Normal University, Shanghai 200241, China

[2]Department of Chemistry, East China Normal University, Shanghai 200062, China

Correspondence to: J.-S. Jiang (E-mail: jsjiang@phy.ecnu.edu.cn)

ABSTRACT: Fe_3O_4/poly (ε-caprolactone)-polyurethane (PCLU) shape memory nanocomposites were prepared by an *in situ* polymerization method. The thermal properties, magnetic properties, and shape memory properties of the nanocomposites were investigated systematically. The results showed that the Fe_3O_4 nanoparticles were homogeneously dispersed in the PCLU matrix, which ensured good shape memory properties of nanocomposites in both hot water and an alternating magnetic field ($f = 45$ kHz, $H = 29.7$ kA m^{-1}/36.7 kA m^{-1}). The nanocomposites started to recover near 40°C, which is slightly higher than body temperature. Thus, they would not change their deformed shape during the implanting process into the human body. Considering potential clinical applications, 45°C was chosen as shape recovery temperature which is slightly higher than 37°C, and the nanocomposites had high shape recovery rate at this temperature. With increasing content of Fe_3O_4 nanoparticles, the shape memory properties of the nanocomposites in an alternating magnetic field increased and the best recovery rate reached 97%, which proves that this kind of nanocomposites might be used as potential magnetic sensitive shape memory materials for biomedical applications. © 2012 Wiley Periodicals, Inc. J. Appl. Polym. Sci. 000: 000–000, 2012

KEYWORDS: polyurethanes; nanocomposites; shape memory; Fe_3O_4 nanoparticles

Received 13 October 2011; accepted 20 January 2012; published online

DOI: 10.1002/app.36849

INTRODUCTION

Shape memory polymers (SMPs) are so intelligent materials that they have been widely concerned in the past decades. The majority of pure SMPs is thermal sensitive that they respond thermal heating (hot liquid or gas) to recover their original shape by releasing the mechanical energy exerted on the material during deformation.[1,2] In view of their advantages, SMPs have been used in various fields such as sensors,[3,4] packaging materials,[5] textiles,[6] and so on. Since Lendlein et al.[7] synthesized a biodegradable polymer and proved its potential applications in animal body, biodegradable SMPs have become a new class of smart polymer materials for biomedical applications, which are used as drug delivery systems,[8] stents, and implants.[9,10]

However, it is not suitable enough to realize the shape memory effect by direct heating in human body. Thus, inductive heating will be a solution. Many researches have been done to realize the shape memory effect by heating from inside particles of SMPs including carbon nanotubes,[11,12] carbon naonofibers,[13] and magnetic particles.[14–17] Among them, magnetic particles, such as iron (II,III) oxide (Fe_3O_4) and nickel zinc ferrite ferromagnetic particles,[17] have the most possibilities to be used in clinical applications. Mohr et al.[14] had incorporated magnetic iron (III) oxide particles into polyetherurethane (TFX) and multiblock copolymer (PDC) with poly(*p*-dioxanone) and poly(ε-caprolactone) (PCL) thermoplastic shape-memory polymers. The shape memory effect of both composite systems were initiated by inductive heating in an alternating magnetic field ($f = 258$ kHz, $H = 30$ kA m^{-1}). Razzaq et al.[15,16] studied the electrical and magnetic properties of magnetite (Fe_3O_4) filled polyurethanes and proved that heat was generated by power loss of magnetic particles. Until now, there have been limited kinds of magnetic SMPs reported such as iron microparticles/polyalkenamer composites,[18] iron(III) oxide/crosslinked oligo(ε-caprolactone) dimethacrylate nanocomposites,[19] iron(III) oxide/TFX nanocomposites,[14] iron (III) oxide/PDC nanocomposites,[14] Fe_3O_4/poly(D,L-lactide) nanocomposites,[20] Fe_3O_4/MM4510 composites,[15] NdFeB/nanoclay/crosslinked low-density polyethylene nanocomposites,[21] and nickel zinc ferrites/MP5510.[17] Therefore, it is necessary to explore more kinds of noncontact-induced SMPs to meet the potential demands of applications.

Considering the potential clinical applications, the magnetic shape memory nanocomposites should meet some basic requirements to reduce the pain of patients. First, the materials should

be safe and nontoxic. Second, the shape recovery temperature must be slightly higher than body temperature. Lastly, the shape recovery rate must be high. Nowadays, many scientists are trying to adjusting the shape recovery temperature at 37°C, and some successful cases have been reported.[10,22] Nevertheless, it is unsuitable enough to obtain the original shape at 37°C. For example, if an implant whose shape recovery temperature is 37°C is placed exactly in human body through operation, it will deploy too quickly that we even have little time to deal with the wound. Thus, it cannot exert its unique function. Also, the shape recovery temperature cannot be too high. Otherwise, the normal cells or tissues will be injured. Therefore, the shape recovery temperature had better several degrees higher than 37°C. In addition, the starting temperature of a shape recovery process must be higher than 37°C as well so that the shape memory materials will not change their deformed shape during the process of implanting to human body. Presently, few SMPs with magnetic fillers can reach the temperature a little bit higher than 37°C and have high shape recovery rate at the same time. Therefore, many efforts should be paid to invent biomedical magnetic shape memory composites. In view of this aim, we use in situ polymerization method to incorporate Fe_3O_4 nanoparticles in poly(ε-caprolactone)-polyurethane (PCLU). As Fe_3O_4 nanoparticles have a few good properties such as biocompatibility, nontoxicicity, and high magnetism, it is a good choice to use them as embedded fillers. Besides, through chemical coprecipitation method, it is easily to obtain a large quantity of nanoparticles. As is known to all, PCLU is an outstanding segmented SMP.[23] PCL is a well-known biodegradable polymer in the extensive biomedical applications because of its nontoxic and biocompatibility. The PCL segment of PCLU is highly crystalline at room temperature, and the degree of microphase separation of PCLU is high, which ensures the good shape memory properties. To the best of our knowledge, such a kind of Fe_3O_4/PCLU magnetic sensitive shape memory nanocomposite has not been reported yet. The mechanical, thermal, magnetic, and shape memory properties of the nanocomposites were systematically investigated.

EXPERIMENTAL

Materials

ε-Caprolactone (CL, 99%) and 4,4′diphenylmethane diisocyanate (MDI, 98%) were purchased from Alfa Aesar and used without further purification. The other related chemicals were purchased from local agent companies. They were listed as followed: 1,4-butanediol (BDO, A.R), stannous octotate [$Sn(Oct)_2$, 95%], dimethylformamide (DMF, A.R), ethylene glycol (EG, A.R), hexane(A.R), toluene(A.R), ferrous sulfate ($FeSO_4{\cdot}7H_2O$, A.R), ferric chloride ($FeCl_3{\cdot}\ 6H_2O$, A.R), sodium hydroxide (NaOH, A.R), and γ-aminopropyltriethoxysilane (KH-550). 1,4-Butanediol (BDO) was dehydrated with 4 Å molecular sieves for 2 days. DMF and toluene were dried over calcium hydroxide (CaH_2) and distilled before being used.

Preparation of PCL Diol and Fe_3O_4 Nanoparticles

PCL diol was synthesized by ring-opening polymerization of ε-caprolactone monomer with EG as initiator according to the literature procedure.[24]

The synthesis of magnetite nanoparticles was performed by precipitating iron salts ($FeSO_4{\cdot}7H_2O$ and $FeCl_3{\cdot}6H_2O$) with molar ratio of 1 : 2 in alkaline medium as reported.[25] To reduce agglomeration, the Fe_3O_4 nanoparticles were modified by KH-550. First, 10 g Fe_3O_4 nanoparticles were dispersed into 500 mL solution ($V_{Ethanol} : V_{Distilled\ water} = 1 : 1$), and the obtained dispersion was stirred for 30 min. Then, 5 mL KH-550 was added into the dispersion, and the dispersion was stirred for another 4 h. The KH-550 modified Fe_3O_4 nanoparticles were collected by sedimentation with a help of an external magnetic field and washed several times with deionized water and ethanol and dried at 40°C in vacuum for 24 h.

Preparation of Fe_3O_4/PCLU Nanocomposites

Fe_3O_4/PCLU nanocomposites were prepared by in situ polymerization method at molar ratio of PCL : MDI : BDO = 1 : 4 : 3 with different content of Fe_3O_4 nanoparticles. A certain amount of PCL diol was dissolved in an equal volume of DMF and heated at 65°C for 20 min. Subsequently, $Sn(Oct)_2$ (0.1 wt % of PCL diol, g/g) in dried DMF and a given amount of MDI were added into the solution which were stirred for 30 min at 65°C to fully mix and 2 h at 85°C to get the prepolymer. Then, BDO was added into the mixture, and the mixture was stirred at 85°C for 3 h. After that, the surface-modified Fe_3O_4 nanoparticles which were dispersed in DMF via a high frequency ultrasonator for 30 min were added and the mixture was stirred for 2 h. Finally, the prepared nanocomposites were put into a glass plate and dried at 80°C in vacuum for 24 h and at 60°C for 48 h. Thus, the 1 ∼ 2-mm-thick specimens were obtained. The prepared nanocomposites with 0, 10, and 30 wt % of the surface-modified Fe_3O_4 nanoparticles (relative to the monomer mixture) were named as CPF0, CPF1, and CPF3, respectively.

Measurements

The molecular weight of the PCL diol was determined by ^{1}H-NMR (Bruker Unity-500) using a tetramethylsiliane as an internal standard in deuterated chloroform ($CDCl_3$). The structure of CPF0 was tested by ^{1}H-NMR in deuterated dimethyl sulfoxide ($DMSO\text{-}d_6$). Fourier transform infrared (FTIR) spectra of PCL, CPF0, CPF1, and CPF3 were recorded by FTIR spectrosmeter (Nexus 670, Nicolets, USA) using potassium bromide (KBr) pellets. The dispersion of the nanoparticles in the nanocomposites was analyzed using field emission scanning electron microscope (FESEM) (Hitachi, S4800). The crystal structure of PCL, CPF0, CPF1, and CPF3 were characterized by X-ray diffraction (XRD). A Rigaku D/max 2550 X-ray diffractometer with Cu Kα radiation was used. The thermal properties were measured by using a differential scanning calorimetry (DSC) (DSC2910, TA, USA). Indium standard was used for calibration. After erasing the previous thermal history, each specimen (about 10 mg) was heated from −50 to 200°C at the scan rate of 10°C min^{-1} purged with nitrogen. The mechanical properties of the nanocomposites were tested by a universal testing machine (Instron RG 3010 made in China) using a dumbbell-type specimen at room temperature. The magnetization curves of the samples were measured by a vibrating sample magnetometer (VSM 7404, Lake Shore, USA) at room temperature.

Investigation of Shape Memory Properties of Fe_3O_4/PCLU Nanocomposites

The shape memory properties of Fe_3O_4/PCLU nanocomposites were investigated by a method called fold-deploy shape memory test.[26] According to this method, the shape memory properties could be obtained by recording the bending angle.

The specimens of 30 × 10 × 1 mm^3 (length ×width ×thickness) were folded at 60°C followed by quenching into an ice-water bath. The folded samples were reheated at 45°C or placed into an alternating magnetic field ($f = 45$ kHz) (SP-15A Inductive Heating Machine, Shenzhen, China) to recover its original shape. The shape memory test of all samples was repeated for three times. The shape recovery process was recorded by using a digital camera. The changed angles of specimens were recorded. θ_f was the angle of the folded samples after being exposed to room temperature for 5 min, and θ_r was the final angle after one shape recovery process. The shape retention rate (R_f) and shape recovery rate (R_r) were calculated using eqs.(1) and (2).

$$R_f\ (\%) = \frac{180^o - \theta_f}{180^o} \times 100 \quad (1)$$

$$R_r\ (\%) = \frac{\theta_r}{180^o} \times 100 \quad (2)$$

RESULTS AND DISCUSSION

The molecular structures of specimens were confirmed by ^{1}H-NMR and FTIR results. ^{1}H-NMR spectra of PCL and CPF0 and their molecular formulas are shown in Figure 1. The results were in accordance with proposed structures.[27]

PCL [^{1}H-NMR $CDCl_3$ Figure 1(a)]: 7.29 ppm ($CHCl_3$), 4.28 (s, 4H, OCH_2CH_2O on EG), 4.06 (t, $J = 8.5$Hz, 2H, CH_2OCO on PCL), 3.65 (s, 2H, CH_2OH on PCL), 2.35–2.30 (m, 2H, $OCOCH_2$ on PCL), 1.68–1.59 (m, 4H, CH_2 on PCL), 1.42–1.35 (m, 2H, CH_2 on PCL).

CPF0 [^{1}H-NMR DMSO-d_6 Figure 1(b)] : 8.54 ppm (s, NHCOO on MDI), 7.40–7.26 (m, 4H, CH on MDI), 7.12–7.02 (m, 4H, CH on MDI), 4.22–4.16 (br, 2H, $OCOCH_2$ on BDO), 4.07–3.91 (m, 2H, CH_2OCO on PCL), 3.88 (s, 2H, CH_2 on MDI), 3.82–3.72 (br, 2H, CH_2O on BDO), 2.50 (DMSO), 2.36–2.18 (m, 2H, CH_2COO on PCL), 1.64–1.45 (m, 4H, CH_2 on PCL), 1.38–1.18 (m, 2H, CH_2 on PCL).

In Figure 1(a), the peaks located at 4.06 ppm and 4.28 ppm are assigned to the protons of CH_2OCO and OCH_2CH_2O, respectively. Because of these characteristic chemical shifts, it is easily to calculate the molecular weight of the PCL diol using following equation.[28]

$$M_n = (I_b/I_g + 1) \times 114 \times 2 + 62 \quad (3)$$

where the I_b and I_g are the areas of peaks *b* and *g*, respectively, 114 is the molar mass of a CL repeat unit and 62 is the total molar mass of the rest part of the molecule. According to eq. 3, it can be calculated that the molecular weight of the PCL diol is about 5000 g mol^{-1}. In Figure 1(b), the signal of urethane NH proton can be observed at 8.54 ppm, which indicates that MDI reacted with PCL.

FTIR spectra of PCL, CPF0, CPF1, and CPF3 are shown in Figure 2(a–d). In Figure 2(a), a broad peak appeared at 3449 cm^{-1} is assigned to OH stretching vibration, and the peak observed at 2951 cm^{-1} and 2864 cm^{-1} are the CH_2 asymmetric and symmetric stretching vibrations.[29] The absorptions at 1730 cm^{-1} is due to C=O bond.[29] As it can be seen at 3346 cm^{-1} in Figure 2(b), it is assigned to NH stretching vibration which indicates the characteristic band of urethane groups.[30] Moreover, the NH deformation peak appears at 1541 cm^{-1}. The absorptions located at 2950 cm^{-1}, 2863 cm^{-1}, and 1730 cm^{-1} are the same peaks described as in Figure 2(a). According to the literature,[29] the characteristic band of NCO groups of MDI should appear at 2255 cm^{-1}. Although in Figure 2(b–d), this peak disappeared. This indicates that the NCO group reacted completely. In contrast to Figure 2(b), the characteristic band of Fe_3O_4 can be seen at 581 cm^{-1} and 630 cm^{-1} which are due to Fe-O

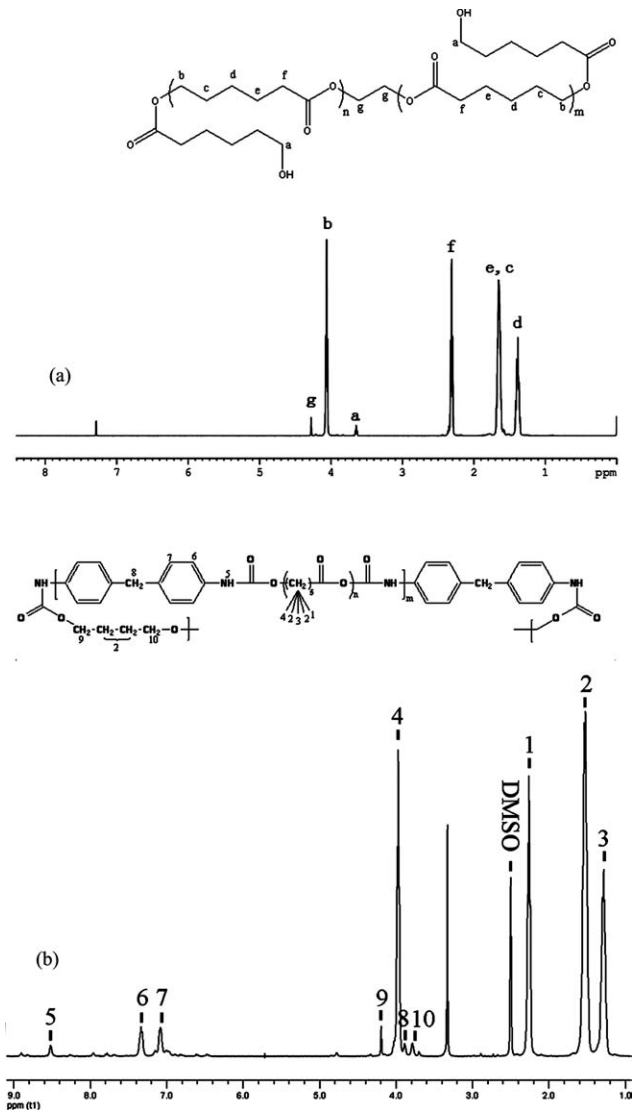

Figure 1. ^{1}H-NMR spectra of PCL diol (a) and CPF0 (b).

Applied Polymer SCIENCE

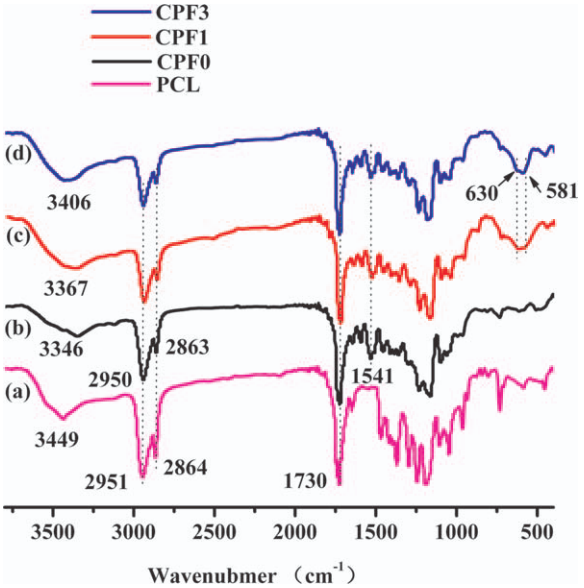

Figure 2. FTIR spectra: (a) PCL diol, (b) CPF0, (c) CPF1, and (d) CPF3. [Color figure can be viewed in the online issue, which is available at wileyonlinelibrary.com.]

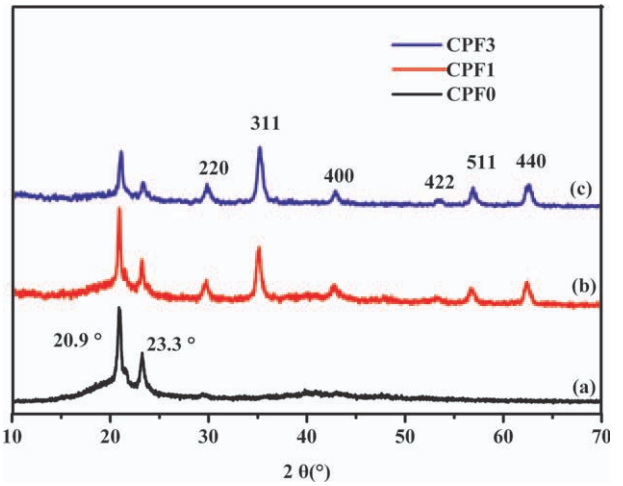

Figure 3. X-ray diffraction pattern of (a) CPF0, (b) CPF1, and (c) CPF3. [Color figure can be viewed in the online issue, which is available at wileyonlinelibrary.com.]

bond[20] in Figure 2(c) and (d). This demonstrates that the surface of Fe_3O_4 was successfully modified with KH-550. What's more, the NH peak at 3346 cm^{-1} in Figure 2(b) shifts to a higher wave number and becomes broader in Figure 2(c) and Figure 2(d). This may be due to the overlapping of free NH bond of KH-550[31] on the surface of Fe_3O_4 which increases with the addition of Fe_3O_4 nanoparticles. These observed peaks in Figure 2 indicates that the formation of polyurethane and polyurethane nanocomposites were successful.

The crystallization property of each nanocomposite was determined by XRD and DSC test. The typical XRD patterns of CPF0, CPF1, and CPF3 are shown in Figure 3. Two well-defined peaks at $2\theta = 20.9°$ and 23.3° of CPF0 in Figure 3(a) are due to the diffraction of PCL soft segment.[32] Meanwhile, there is a broad peak near $2\theta = 20°$ which suggests that this sample is partially crystallized and the rest are in amorphous state. From Figure 3(b,c), another six diffraction peaks can be seen clearly which are indexed as Fe_3O_4 (JCPDS No.19-0629). The average grain size of Fe_3O_4 particles calculated by the Scherrer formula is about 20 nm. For the diffraction peaks of PCL soft segment do not shift, it may be concluded that the embedded Fe_3O_4 nanoparticles do not result in a change of crystal structure of the polymer matrix. This is further confirmed by DSC analysis. Figure 4 shows DSC second thermogram curves of CPF0, CPF1, and CPF3 in which obvious melting peaks can be seen. The melting temperature (T_m) which is assigned to the melt of crystalline PCL phase and the melting enthalpy (ΔH_m in J/g) obtained from DSC analysis are also summarized in Table I. According to the data, T_m only slightly increases after the incorporation of Fe_3O_4 nanoparticles, and this may be caused by the heat absorption of Fe_3O_4 nanoparticles during the calefactive process. This result means that the incorporation of Fe_3O_4 nanoparticles does not significantly affect the melting temperature of the crystalline PCL phase.[33] As the perfect PCL crystal has a melting enthalpy of 140 J/g,[34] lower enthalpy values of the samples in Table I show that the samples were partially crystallized.

The dispersion of the nanoparticles in polymer matrix is shown in Figure 5. All the pictures are the cross sectional drawings of the nanocomposites. Figure 5(a) and (c) are the secondary electron images (SE), whereas (b) and (d) are backscattered electron images (BSE). The visible bright points in Figure 5(b) and (d) are the Fe_3O_4 particles, and the grey parts are polymer matrix. Furthermore, it can be seen that the Fe_3O_4 particles are uniformly distributed in the matrix of CPF1 on the whole, although some particles may agglomerate during specimen formation. Because there are more Fe_3O_4 nanoparticles in CPF3, the agglomerate is obvious and the dispersion becomes poorer. In addition, there are more protuberances in SE pictures, and the cross sectional surface become more roughness with the increasing Fe_3O_4 contents, which provides the evidence that the

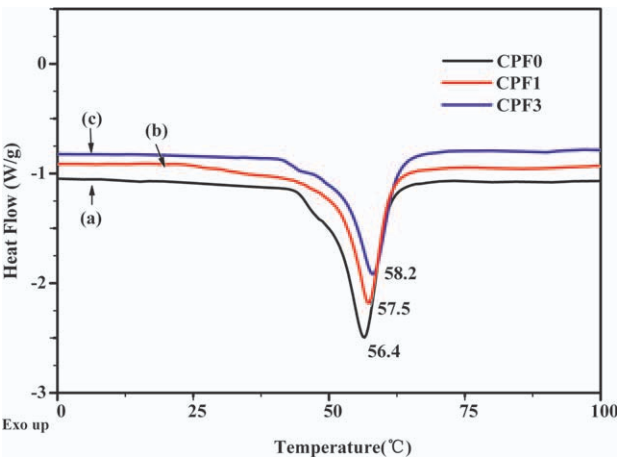

Figure 4. DSC second covers of samples: (a) CPF0, (b) CPF1, and (c) CPF3. [Color figure can be viewed in the online issue, which is available at wileyonlinelibrary.com.]

Table I. DSC Data of Samples: (a) CPF0, (b) CPF1, and (c) CPF3

Sample	T_m (°C)	ΔH_m (J/g)
CPF0	56.4	69.9
CPF1	57.5	67.1
CPF3	58.2	60.6

regularity of polymer matrix is destroyed by the Fe_3O_4 particles to some extent.

Figure 6 illustrates the mechanical properties of specimens, which shows reduced tendency of tensile strength and elongation at break. With the increasing content of Fe_3O_4 nanoparticles, the tensile strength decreases from 23 to 13.8 MPa and the elongation at break decreases from 35.6 to 14.3%. The higher content of the nanoparticles in the polymer matrix, the more brittle nanocomposites will be. For the presence of the nanoparticles, the motion of coiled molecular chains is resisted and the regularity of polymer matrix reduced. This result is in accordance with the FESEM studies.

The magnetic properties can be obtained from magnetic hysteresis loops showed in Figure 7. All samples have low magnetic coercivity and are nearly superparamagnetism. The saturation magnetization of pure Fe_3O_4 nanoparticles is 53.6 emu/g, which is lower than bulk for the nanometer size effect.[35] When the percentage of Fe_3O_4 nanoparticles increases, the saturation magnetization of nanocomposites also increases. The saturation magnetizations of nanocomposites CPF1 and CPF3 are 3.4 emu/g and 10.0 emu/g, respectively. Those data approach theoretical values.

The shape memory properties of polyurethane and its nanocomposites were studied both in hot water and an alternating

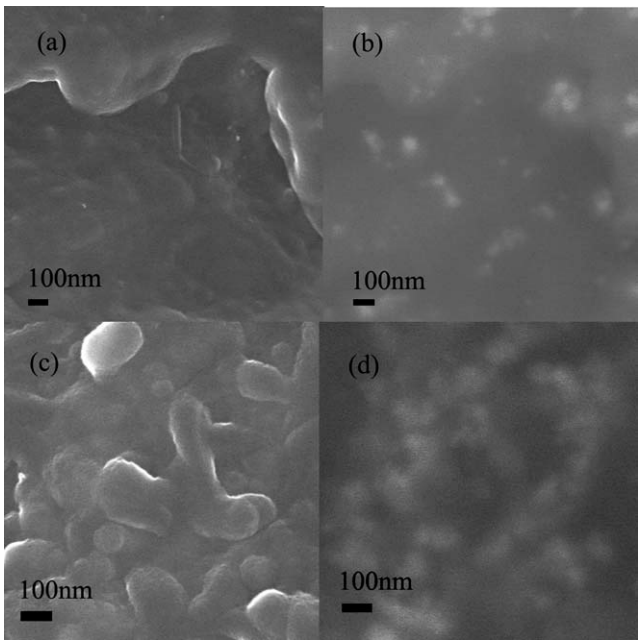

Figure 5. FESEM photos: (a) CPF1 (SE), (b) CPF1 (BSE), (c) CPF03(SE), and (d) CPF3 (BSE).

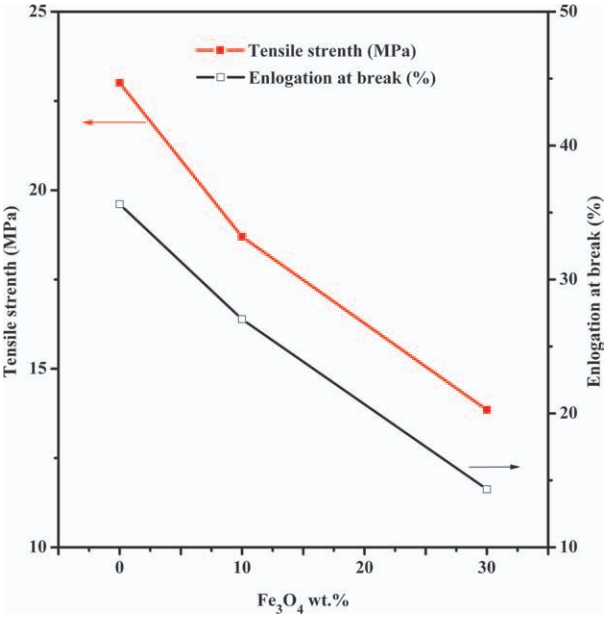

Figure 6. The mechanical properties of specimens. [Color figure can be viewed in the online issue, which is available at wileyonlinelibrary.com.]

magnetic field. Because the T_m of each specimen is slightly lower than 60°C, 60°C is selected as the deformation temperature which cannot only guarantee the fully melting of PCL segment but also avoid the flow of the samples when overheating. In the process for fold-deploy shape memory test, the folded samples were firstly exposed in room temperature for 5 min. There was no obvious change of specimens, and the shape retention rate was nearly about 99%. Figure 8 shows the shape recovery rate of CPF0 and Fe_3O_4/PCLU nanocomposites at different temperatures in hot water. All samples show the lowest recovery temperatures near T_m-15°C. This is consistent with Ping's result[24] in which the lowest recovery temperature of polyurethane based on the PCL soft segment and 2,4-toluene diisocynate-ethylene glycol hard segment was lower than T_m by 10–15°C. As shown in the graph, the shape recovery process starts

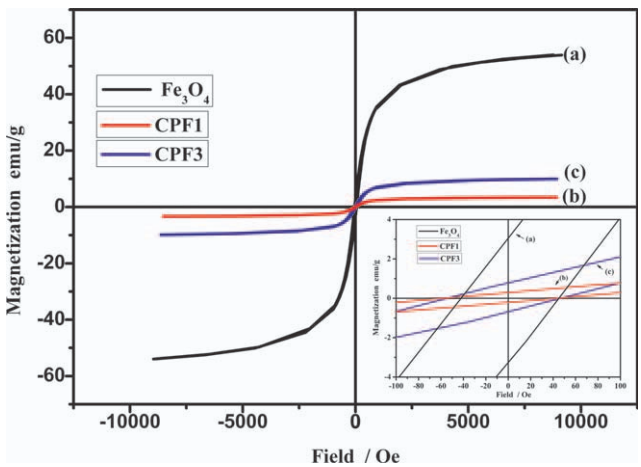

Figure 7. Magnetic hysteresis loops at room temperature of (a) Fe_3O_4, (b) CPF1, and (c) CPF3. [Color figure can be viewed in the online issue, which is available at wileyonlinelibrary.com.]

Applied Polymer SCIENCE

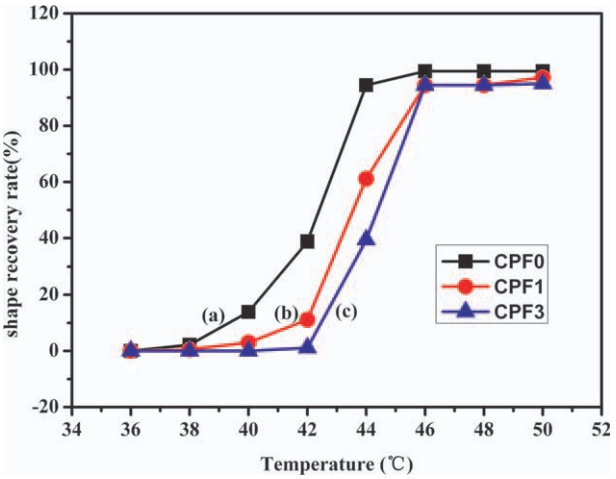

Figure 8. Shape recovery rate of CPF0, Fe_3O_4/PCLU nanocomposites at different temperatures in hot water. [Color figure can be viewed in the online issue, which is available at wileyonlinelibrary.com.]

Figure 9. The process of shape memory recovery of CPF1 in 45°C hot water. [Color figure can be viewed in the online issue, which is available at wileyonlinelibrary.com.]

at a temperature near T_m-15°C and takes place over a narrow temperature range for the strong inner stress frozen in the specimen released quickly. When the temperature is higher than 46°C, the shape recovery rate of three specimens reaches an almost same high value. Therefore, we selected 45°C as a thermal transition temperature (T_{trans}), which is slightly higher than body temperature and will not too high to damage the cells. When specimens were placed into 45°C water, they exhibited good shape memory properties. A typical shape recovery process of CPF1 is shown in Figure 9. The shape recovery rate and shape recovery time of all samples are summarized in Table II. According to Table II, shape recovery rate decreases with the increasing content of Fe_3O_4, whereas shape recovery time enhances. The reason may be that the Fe_3O_4 particles destroy the integrality of molecule chain which is proved in FESEM photos, and they restrict the thermo-motions of chain segments of the polymer during shape recovery process as well. Thus, the nanocomposites could not show good shape memory properties as pure polymer did. The shape memory nanocomposites can gain high shape recovery rate at 45°C. In comparison with most nanocomposites filled with magnetic fillers, our specimens show a relatively lower transition temperature, which may be used as potential biomedical shape memory materials.

It is noteworthy in Figure 8 that CPF0 starts to recover at the temperature of 38°C, which is only one degree higher than 37°C. Hence, this material is not suitable enough to be used in clinical application because it may have little shape change during the implanting process into human body. However, these starting temperatures of nanocomposites rise with the increasing content of Fe_3O_4 particles which are 40°C and 42°C, respectively. These phenomena indicate that there should be sufficient time to finish implanting the shape memory naonocomposites into human body. The shape memory nanocomposites will not change their deformed shape during the process. However, they can regain

Table II. Shape Memory Properties of CPF0 and Fe_3O_4/PCLU Nanocomposites in 45°C Hot Water

Specimens	Shape recovery rate (%)	Recovery time (s)
CPF0	98.3 ± 0.56	17 ± 1.73
CPF1	94.4 ± 0.85	18 ± 1.53
CPF3	90.0 ± 0.32	26 ± 2.31

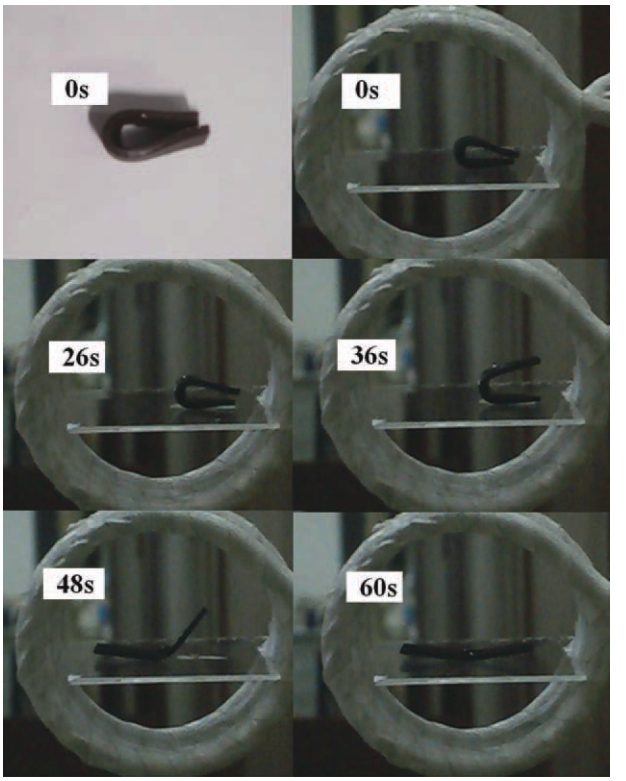

Figure 10. A typical process of shape memory recovery of CPF1 in a magnetic field (f = 45 kHz, H = 29.7 kA m^{-1}).

Table III. Shape Memory Properties of Fe_3O_4/PCLU Nanocomposites in Different Magnetic Fields

Specimens	Magnetic field	Magnetic field response time (s)	Recovery time (s)	Shape recovery rate (%)
CPF1	$f = 45$ kHz, $H = 29.7$ kA m^{-1}	20 ± 2.08	40 ± 2.52	93.33 ± 0.32
CPF3	$f = 45$ kHz, $H = 29.7$ kA m^{-1}	4 ± 0	30 ± 2.65	95.56 ± 0.32
CPF1	$f = 45$ kHz, $H = 35.7$ kA m^{-1}	7 ± 0.58	50 ± 1.53	94.44 ± 0.64
CPF3	$f = 45$ kHz, $H = 35.7$ kA m^{-1}	2 ± 0	26 ± 1.15	97.22 ± 0.85

their original shape by the stimulation outside body. Thus, the shape memory behaviors of magnetic nanocomposites in an alternating magnetic field are expected. Because of the hysteresis loss and eddy current losses in an alternating magnetic field, embedded magnetic particles in polymer matrix will generate heat which can induce shape memory effect.[16] In this article, we studied the shape memory properties of the samples under such a given alternating magnetic field ($f = 45$ kHz, $H = 29.7$ kA·m^{-1}). A shape recovery process of CPF1 is illustrated in Figure 10. The folded sample is shown as well. In the first 20s, the sample (CPF1) does not exhibit an obvious change. The reason is that the heat produced by magnetic particles is not enough that the temperature of sample cannot reach T_{trans}. When the temperature is near or higher than T_{trans}, the sample quickly reaches its original shape. The shape recovery rate and shape recovery time of all samples are summarized in Table III. With increasing content of nanoparticles, the samples in the same alternating magnetic field could produce more heat to let the temperature reach or near T_{trans} that the magnetic field response time and recovery time decrease while the shape recovery rate enhances. The shape recovery rate of CPF1 in the alternating magnetic field is lower than that in the water bath but there is an opposite phenomenon in CPF3. If temperature of a sample can reach its T_{trans} quickly, the internal stress frozen in deformation may impel the sample to recover faster and will be influenced less by stress relaxation and creep. So the recovery rate of the samples with more nanoparticles is relatively higher. It can be concluded that more nanoparticles in polymer matrix can lead less magnetic field response time and less stress relaxation that samples can get higher shape recovery rate. During the shape recovery process, it was observed that CPF1 started to recover at the temperature of 41°C. When it fully recovered, the temperature reached 50°C. CPF3 showed the similar phenomenon that the temperatures were 43°C and 51°C, respectively. With more Fe_3O_4 particles, CPF3 can easily reach a high temperature. The starting temperatures of shape memory nanocomposites in the alternating magnetic field are near the values in hot water. Therefore, these materials are considered as suitable implantable materials. Through adjusting the current, the intensity of the alternating magnetic field can be changed. Hence, the shape memory behavior of the nanocomposites were tested in a higher intensity magnetic field ($f = 45$ kHz, $H = 35.7$ kA m^{-1}). The data are also listed in Table III, which show a lower recovery time and higher shape recovery rate. Considering the noncontact-inducing shape memory behavior of the nanocomposites in an alternating magnetic field, this kind of materials may be used as potential magnetic sensitive shape memory materials in clinical applications.

CONCLUSIONS

The magnetic sensitive shape memory polyurethane nanocomposites with various contents of Fe_3O_4 nanoparticles were successfully synthesized by in situ polymerization method. This kind of nanocomposites exhibited good shape memory behavior in both water bath and alternating magnetic field. The starting temperatures were near 40°C so that these materials were considered as ideal implantable materials. The shape memory composites exhibited high shape recovery rate at 45°C, which was slightly higher than body temperature. With the increasing percentage of Fe_3O_4, the shape recovery time decreased. The shape recovery rate of samples was over 94% with the highest at 97% in the alternating magnetic field ($f = 45$ kHz, $H = 35.7$ kA m^{-1}). These nanocomposites are expected to be used as potential magnetic sensitive shape memory materials for biomedical applications.

ACKNOWLEDGMENTS

This work was supported by the National Natural Science Foundation of China (Grant No. 21173084), Shanghai Nanotechnology Promotion Center (Grant No.0852 nm03200) and Equipment Sharing Platform of ECNU.

REFERENCES

1. Behl, M.; Lendlein, A. *Mater. Today* **2007,** *10*, 20.
2. Behl, M.; Lendlein, A. *Soft Matter* **2007,** *3*, 58.
3. Kunzelman, J.; Chung, T.; Mather, P. T.; Weder, C. *J. Mater. Chem.* **2008,** *18*, 1082.
4. Gall, K.; Kreiner, P.; Turner, D.; Hulse, M. *J. Microelectromech. S.* **2004,** *13*, 472.
5. Behl, M.; Razzaq, M. Y.; Lendlein, A. *Adv. Mater.* **2010,** *22*, 3388.
6. Hu, J. L.; Chen, S. J. *J. Mater. Chem.* **2010,** *20*, 3346.
7. Lendlein, A.; Langer, R. *Science* **2002,** *296*, 1673.
8. Xiao, Y.; Zhou, S. B.; Wang, L.; Zheng, X. T.; Gong, T. *Compos. Part B Eng.* **2010,** *41*, 537.
9. Xue, L.; Dai, S. Y.; Li. Z. *Biomaterials* **2010,** *31*, 8132.
10. Ajili, S. H.; Ebrahimi, N. G.; Soleimani, M. *Acta. Biomater.* **2009,** *5*, 1519.
11. Xiao, Y.; Zhou, S. B.; Wang, L.; Gong, T. *ACS Appl. Mater. Interf.* **2010,** *2*, 3506.
12. Ni, Q. Q.; Zhang, C. S.; Fu, Y. Q.; Dai, G. Z.; Kimura, T. *Compos. Struct.* **2007,** *81*, 176.
13. Gunes, I. S.; Jimenez, G. A.; Jana, S. C. *Carbon* **2009,** *47*, 981.

14. Mohr, R.; Kratz, K.; Weigel, T.; Lucka-Gabor, M.; Moneke, M.; Lendlein, A. *PNAS* **2006,** *103*, 3540.
15. Razzaq, M. Y.; Anhalt, M.; Frormann, L.; Weidenfeller, B. *Mater. Sci. Eng. A* **2007,** *471*, 57.
16. Razzaq, M. Y.; Anhalt, M.; Frormann, L.; Weidenfeller, B. *Mater. Sci. Eng. A* **2007,** *444*, 227.
17. Buckley, P. R.; McKinley, G. H.; Wilson, T. S.; Small, W., IV; Benett, W. J.; Bearinger, J. P.; McElfresh, M. W.; Maitland, D. J. *IEEE T. Bio. Med. Eng.* **2006,** *53*, 2075.
18. Cuevas, J. M.; Alonso, J.; German, L.; Iturrondobeitia, M.; Laza, J. M.; Vilas, J. L.; Le'on, L. M. *Smart Mater. Struct.* **2009,** *18*, 075003.
19. Razzaq, M. Y.; Behl, M.; Kratz, K.; Lendlein, A. *Mater. Res. Soc. Symp. Proc.* **2009,** *1140*, 185.
20. Zheng, X. T.; Zhou, S. B.; Xiao, Y.; Yu, X. J.; Li, X. H.; Wu, P. Z. *Colloid. Surf. B* **2009,** *71*, 67.
21. Golbang, A.; Kokabi, M. *Adv. Mater. Res.* **2010,** *123–125*, 999.
22. Hearon, K.; Gall, K.; Ware, T.; Maitland, D. J.; Bearinger, J. P.; Wilson, T. S. *J. Appl. Polym. Sci.* **2011,** *121*, 144.
23. Li, F. G.; Hou, J. N.; Zhu, W.; Zhang, X.; Xu, M.; Luo, X. L.; Ma, D. Z.; Kim, B. K. *J. Appl. Polym. Sci.* **1996,** *62*, 631.
24. Ping, P.; Wang, W. S.; Chen, X. S.; Jing, X. B. *Biomacromolecules* **2005,** *6*, 587.
25. Gan, Z. F.; Jiang, J. S.; Yang, Y.; Du, B.; Qian, M.; Zhang, P. *J. Biomed. Mater. Res. A* **2008,** *84A*, 10.
26. Liu, Y. Y.; Han, C. M.; Tan, H. F.; Du, X. W. *Mater. Sci. Eng. A* **2010,** *527*, 2510.
27. Zia, K. M.; Barikani, M.; Zuber, M.; Bhatti, I. A.; Sheikh, M. A. *Carbohydr. Polym.* **2008,** *74*, 149.
28. Wang, W. S.; Ping, P.; Chen, X. S.; Jing, X. B. *Eur. Polym. J.* **2006,** *42*, 1240.
29. Zia, K. M.; Bhatti, I. A.; Barikani, M.; Zuber, M.; Bhatti, H. N. *Carbohydr. Polym.* **2009,** *76*, 183.
30. Zhu, Y.; Hu, J. L.; Yeung, K. *Acta. Biomater.* **2009,** *5*, 3346.
31. Xie, N.; Jiao, Q. J.; Zang, C. G.; Wang, C. L.; Liu, Y. Y. *Mater. Des.* **2010,** *31*, 1676.
32. Chen, S. J.; Hu, J. L.; Liu, Y. Q.; Liem, H.; Zhu, Y.; Meng, Q. H. *Polym. Int.* **2007,** *56*, 1128.
33. Yu, X. J.; Zhou, S. B.; Zheng, X. T.; Guo, T.; Xiao, Y.; Song, B. T. *Nanotechnology* **2009,** *20*, 235702.
34. Yang, D.; Huang, W.; Yu, J. H.; Jiang, J. S.; Zhang, L.; Xie, M. R. *Polymer* **2010,** *51*, 5100.
35. Hu, M.; Ji, R. P.; Jiang, J. S. *Mater. Res. Bull.* **2010,** *45*, 1811.